Research Article Vol. 33, No. 4 / 24 Feb 2025 / Optics Express 8203
Optics EXPRESS

Phononically shielded multi-wavelength photonic-crystal membrane for cavity quantum optomechanics

HANBING LI,[1,2] DOUDOU WANG,[1,2] QUANSEN WANG,[1,2] QIANG ZHANG,[1,2] AND YONGMIN LI[1,2,*]

[1]State Key Laboratory of Quantum Optics Technologies and Devices, Institute of Opto-Electronics, Shanxi University, Taiyuan 030006, China
[2]Collaborative Innovation Center of Extreme Optics, Shanxi University, Taiyuan, Shanxi 030006, China
[*]yongmin@sxu.edu.cn

Abstract: We propose and design a stoichiometric silicon-nitride membrane resonator featuring high reflectivity at multi-wavelengths and high mechanical quality factors. The membrane resonator has a thickness of 100 nm and 2D-photonic and phononic crystal patterns. By designing concentric holes of suitable radius on both sides of the membrane, high reflectivity at multi-wavelengths can be achieved. In particular, the simulation shows that high reflectivity can be realized at telecommunications wavelengths and alkaline atomic absorption lines, achieving reflectivity of 99.76% at 852 nm, 99.98% at 1054 nm, and 99.96% at 1566 nm, respectively. The designed device can find useful applications in cavity optomechanical systems to realize quantum frequency conversion and precise quantum measurements, and other quantum information processing tasks.

1. Introduction

Cavity optomechanics exploits the radiation pressure interaction between the optical field and the mechanical resonators [1,2]. It has found wide applications, from fundamental quantum physics to quantum measurements and quantum information processing [3]. By circulating optical fields in cavities, the interaction between the light and mechanical resonators can be greatly enhanced. The confining of the optical fields in cavities also enables a number of interesting physical phenomena ranging from the motional ground state cooling of the resonator to optomechanically induced transparency, squeezing and entanglement of light fields, and mechanical oscillators, transversion between microwave and optical light, and quantum sensing, etc. The dielectric membrane resonators based cavity optomechanics system, where the optical and mechanical resonators can be independently designed and optimized, have attracted a lot of interests [4].

Silicon nitride (SiN) membranes, feature low optical absorption and high mechanical quality factors, making them widely used in many membrane-in-the-middle cavity optomechanical systems. By designing photonic crystals structures [5–8] on the membrane, high reflectivity can be achieved. In this way, the membrane can act as both the resonator and one of the end mirrors in the optomechanical system. In contrast to the membrane-in-the-middle system, such a configuration can enable a compact optomechanical system and enhance the optomechanical coupling rate g_0.

Recently, several experiments have explored the photonic crystal membranes in cavity optomechanics [9–14]. Moura et al. [15] presented centimeter-scale suspended photonic crystal mirrors and obtained reflectivity higher than 90% at 1550 nm. Enzian et al. [16] presented a stoichiometric silicon-nitride membrane, which combined both the photonic and phononic crystal structures and has a reflectivity of 99.89% and a mechanical quality factor of 2.9×10^7 at room temperature. Agrawal et al. [17] realized a 99% reflectivity focusing metamirror using

#550826 https://doi.org/10.1364/OE.550826
Journal © 2025 Received 2 Dec 2024; revised 30 Jan 2025; accepted 9 Feb 2025; published 18 Feb 2025

Optics EXPRESS

non-periodic photonic crystal patterning in a Si_3N_4 membrane. Very recently, Zhou et al. [18] reported ultrahigh reflectivity photonic crystal membranes, which can reach reflectivity up to 99.982% using a hexagonal lattice. They found that the hexagonal lattices have a wider spectral reflection range and reflectance and less susceptibility to the manufacturing imperfections in comparison to the square lattices.

At present, most of the research of the photonic crystal membranes focus on the realization of high reflectance from a single wavelength [15–18]. Extending the high reflectance ability from a single wavelength to a multiple wavelength range is useful to enrich the toolbox of the cavity optomechanical systems. For instance, a two-cavity optomechanical system can be constructed using two-wavelength photonic crystal membranes to achieve quantum frequency conversion between the quantum memory wavelength at 800 nm band and telecom wavelength at 1.5 micron.

In this work, we propose and design a stoichiometric silicon-nitride membrane resonator featuring high reflectivity at multiple wavelengths and high mechanical quality factor. The membrane resonator has a thickness of 100 nm and 2D-photonic and phononic crystal patterns. By designing concentric holes of suitable radius on both sides of the membrane, high reflectivity at multi-wavelengths is achieved. In particular, the simulation results show that high reflectivity can be realized at telecommunication wavelengths and alkaline atoms absorption lines, with reflectivity of 99.76% at 852 nm, 99.98% at 1054 nm, and 99.96% at 1566 nm, respectively. The designed devices can be exploited to construct a compact optomechanical system with a high optomechanical coupling rate, which can find potential applications in cavity optomechanical systems to realize quantum frequency conversion, preparation of nonclassical optical and mechanical states, as well as ultrasensitive quantum measurement.

This article is organized as follows: In section 2, we present the design and simulation results of the membrane resonator in detail. In section 3, we present the potential applications of the designed phononically shielded multi-wavelength photonic crystal membrane on cavity quantum optomechanics. Finally, we give a summary.

2. Phononically shielded multi-wavelength photonic-crystal Si_3N_4 membrane resonator

2.1. Design and parameters

The basic structures of our Si_3N_4 membrane resonator consist of both the photonic crystal and the phononic crystal patterns [16–20]. Based on this structure, we design and optimize the phononic crystal and photonic crystal structures to enable the membrane resonator to possess both high mechanical quality factor and high reflectivity at multi-wavelength. There are some overall guiding principles for the device design. Firstly, the reflectances of the maximum and minimum target wavelengths are simulated to obtain the benchmark parameters of lattice constants and hole radius. Next, the parameters are fine tuned to optimize the reflectivity at the specified wavelengths. More precisely, as the lattice constant increases, the hole radius should increase accordingly in general to roughly find the target wavelength position and the maximum reflectivity. For the fixed lattice constant, the increase of the hole radius will shift the maximum reflectance to a shorter wavelength.

As shown in Fig. 1, the squared Si_3N_4 membrane has a thickness of 100 nm and a side length of 3.8 mm, and it is suspended on top of a 10 × 10 mm Si substrate with thickness of 500 μm. The phonon crystal consists of a honeycomb lattice of circular holes with lattice constant 173.2 μm and 0.92 GPa pre-tension. The radius of the dominant circular holes is 45 μm, and the radius of the secondary holes surrounding the photonic crystal is 23.85 μm. A circular geometric defect with a radius of 95 μm is introduced in the center of the phonon crystal structure to localize the vibration of the mechanical mode in the bandgap of phonons crystal. The defect contains the photonic crystal structure that comprises a hexagonal lattice of concentric horn like holes with a

Optics EXPRESS

lattice constant of 1695 nm. The radii of the concentric holes are 33 and 622.2 nm, respectively, and the depths of the holes are 30 and 70 nm, respectively, as shown in Fig. 2(a).

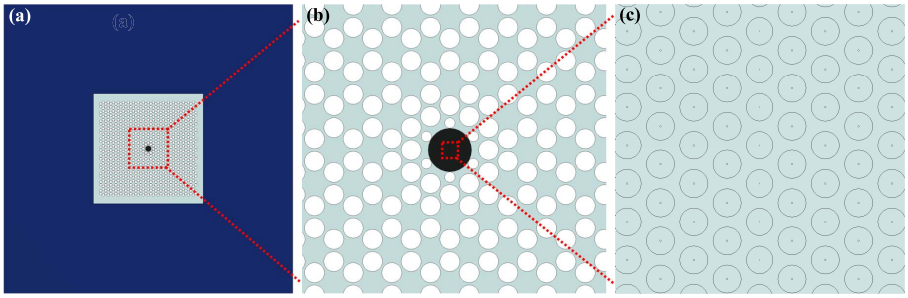

Fig. 1. Schematic diagram of the phononically shielded multi-wavelength photonic-crystal Si_3N_4 membrane resonator. (a) The blue region denotes the silicon frame, and the light grey-green region represents the Si_3N_4 membrane, which comprises two kinds of structures: the centered hexagonal photonic crystal structure (black) and the surrounded honeycomb phononic crystal structure (light grey-green). (b) Zoom of the structure of the phononic crystal. (c) Zoom of the photonic crystal structure.

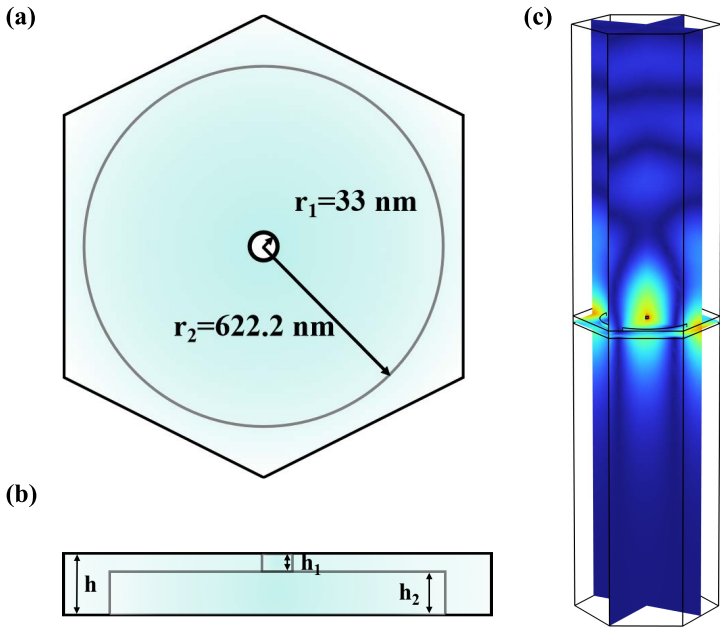

Fig. 2. (a) Three-dimensional top view of a single unit cell of the photonic crystal. The radius of the small hole for the photonic crystals is r_1 = 33 nm and that of the large hole is r_2 = 622.2 nm. (b) Front view of a single unit cell. The thickness of the cell is h = 100 nm, and the two holes have the different thickness of h_1 = 30 nm, h_2 = 70 nm. (c) The electric field distribution diagram using the COMSOL plane wave simulation.

Optics EXPRESS

2.2. Simulation

Numerical simulations of both the optical and mechanical characteristics of the membrane resonator are performed using the finite element method (FEM) with COMSOL Multiphysics [21].

2.2.1. Optical characteristics of the photonic crystal structures

We simulate the reflectance of the multi-wavelength photonic crystal structures by using the physical field of the electromagnetic wave frequency domain (EWFD) of the COMSOL. A single unit cell with periodic boundaries that models an infinite array and a plane-wave input to the photonic crystal structures are employed in the simulation model. The simulation uses the parameters mentioned above and the index of refraction of Si_3N_4: $Re(n) = 1.98$ and $Im(n) = 5 \times 10^{-6}$ [22]. Moreover, the port boundary conditions for transmitting the incident waves, absorbing the transmitted and reflected waves are set [20].

Figure 3 shows the reflectivity of the photonic crystal structure of the membrane as a function of the wavelength simulated by the FEM. Here, the side of the photonic crystal structures with a smaller hole radius is set as the entrance port. From Fig. 3, we can find that the photonic crystal structure of the membrane exhibits near-unity high reflectivity at multiple wavelengths. The reflectivity is 99.76% at 852 nm, 99.98% at 1054 nm, and 99.96% at 1566 nm, respectively. The wavelengths of 852 and 1566 nm fall in the telecom windows. The wavelength of 1054 nm lies in the waveband of free-space optical communication. Note that the wavelength of 852 nm is also the D2 line of Cs atoms, which is suitable for quantum memory and long-distance quantum communication.

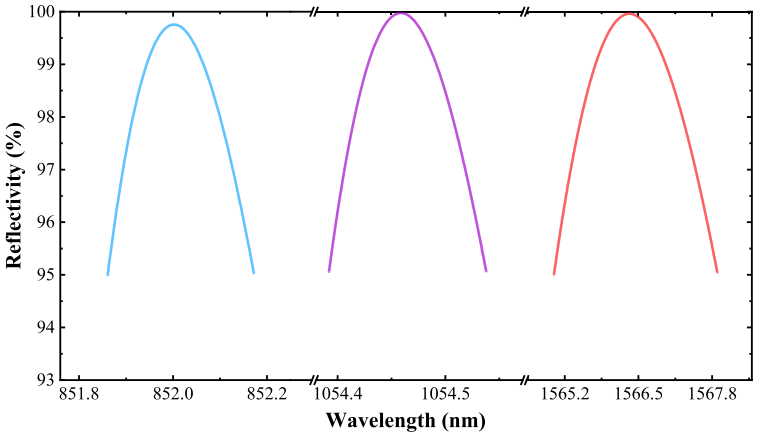

Fig. 3. The reflectivity of the photonic crystal structure of the SiN membrane as a function of the wavelength simulated by the FEM. A plane wave at normal incidence and infinite extension of the photonic crystal structure is adopted. The reflectivity reaches 99.76% at 852 nm, 99.98% at 1054.5 nm, and 99.96% at 1566.3 nm, respectively.

The photonic crystal structure is asymmetrical in the direction perpendicular to the membrane surface. Therefore, the characteristics of reflectivity (transmission) are not identical when the light field impinges on the photonic crystal structure membrane from different sides. Figure 3 shows the reflectivity and transmission when the plane wave enters the membrane from the upper side (Fig. 2(b)). If the plane wave incidents on the membrane from the below side, the reflectivity is 40.49% at 852 nm, 99.98% at 1054.5 nm, and 99.97% at 1566.3 nm, respectively. For some applications, the light fields will incident on the membrane from both sides (please refer to Sec. 3). In this case, we can select the appropriate planes of the light incidence to ensure

Optics EXPRESS

high reflectivity for specified wavelengths. For instance, the light at 852 nm can be incident on the membrane from the upper side, whereas the light at 1566 nm can be impinged from the other side.

The physical mechanism underlying the high reflectivity is that photonic crystal structures give rise to resonances that couple out-of-plane radiation to in-plane leaky modes, which can be employed to achieve high reflectivity at specified wavelengths [15]. The factors that limit the achievable reflectivity include the lattice constant and hole radius in photonic crystal structure, the thickness and index of refraction of the SiN membrane. In general, for the hexagonal lattice, the maximum reflectivity increases with the membrane thickness and the index of refraction. When the thickness and index of refraction are constant, the lattice constant and hole radius limit the minimum transmittance that can reach the Fano resonance and thus bound the maximum reflectivity. Given the specified wavelengths, the maximum reflectance can be achieved only at the specific lattice constants and hole radius.

2.2.2. Mechanical properties of the membrane resonator

We use the stationary and eigenfrequency to study the mechanical properties of the membrane resonator in COMSOL. The eigenfrequency of the membrane resonator is simulated by the membrane physical field in COMSOL, and the band gap of the phonon crystal is simulated by the solid mechanics physical field [23,24]. The whole structure of the membrane is used to simulate the eigenfrequency. Similar to the reflectivity of the photonic crystal, a single unit cell with periodic boundaries that model an infinite array is employed to simulate the band gap diagram of the phonon crystal. For the physical field of the membrane and the solid mechanics, we choose a three-dimensional model design. By using the parameters of the phonon crystal structures mentioned above and SiN: the Young's modulus of 270 GPa, Poisson's ratio of 0.27, and density of 3200 kg/m^3, we get the mechanical properties of the SiN membrane. In addition, the simulation of the eigenfrequency requires fixed constraint boundary conditions, and the band gap simulation requires both the fixed constraint boundary and periodic boundary conditions [20].

Figure 4(a) depicts the simulated mode shape of the mechanical defect mode we studied, which is the lowest-order mechanical defect mode with the vibration frequency of $\omega_m = 1.29$ MHz. Figure 4(b) depicts the simulated band gap diagram of the phonon crystal structure by parametric sweep, and two band gaps (the light blue region) are visible. The first band gap is relatively broad, ranging from 1.168 to 1.406 MHz, and the second band gap ranging from 2.287 to 2.314 MHz is narrower. It is clear that the vibration frequency of the lowest-order mechanical defect mode resides in the middle of the first band gap. Therefore, this mechanical mode will be immune to the external mechanical vibrations, and a high mechanical quality factor can be achieved.

The mechanical quality factor characterizes the mechanical loss of resonators and is defined as the ratio of the energy stored in the mechanical resonator to the energy lost per unit vibration period [25,26]

$$Q_m = \frac{E_{\text{stored}}}{-\frac{dE_{\text{stored}}}{dt} \cdot T}, \tag{1}$$

where $E_{\text{stored}} = A_0^2 e^{-2t\,\text{Im}(\omega_m)}$. is the mechanical energy stored in the mechanical resonator, and $T = \frac{2\pi}{\text{Re}(\omega_m)}$. is the vibration period. By substituting these two expressions into Eq. (1), we can get

$$Q_m = \frac{\text{Re}(\omega_m)}{2 \cdot \text{Im}(\omega_m)}, \tag{2}$$

where $Re(\omega_m)$ and $Im(\omega_m)$ are the real and imaginary parts of the eigenfrequency, respectively. From Eq. (2), the mechanical quality factor, Q_m is estimated to be 1.08×10^8.

Optics EXPRESS

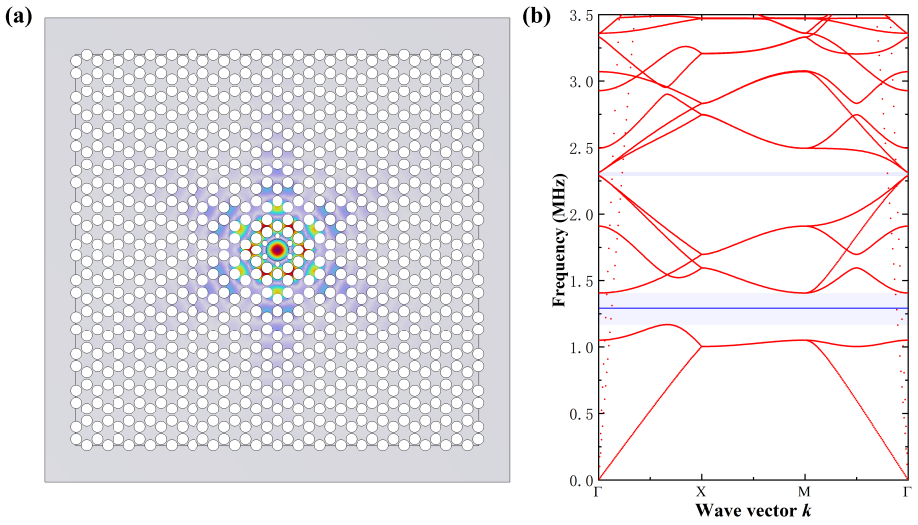

Fig. 4. Mechanical properties of the phononically shielded membrane resonators. (a) Mode shape diagram of the lowest-order mechanical defect modewhich shows the lowest-order mechanical defect mode with a vibration frequency of 1.29 MHz. (b) Band gap diagram of the phonon crystal structure. The light blue region denotes the band gap of the phonon crystal, and the blue line denotes the vibration frequency of the lowest-order mechanical defect mode, which lies in the middle of the phonon gap band.

In addition, we can estimate the effective mass m_{eff} of the designed resonator via the mode shape of the membrane resonator [16]

$$m_{\text{eff}} = \iint_S \left(dx\, dy\, \rho(x,y) \left| \frac{D(x,y)}{D(x_0,y_0)} \right|^2 \right), \tag{3}$$

where $\rho(x,y)$ and d are the density and thickness of the membrane resonator, $z(x,y)$ is the out-of-plane displacement of the mechanical mode, $D(x,y)/D(x_0,y_0)$ denotes the normalized displacement field of the mechanical mode that can be obtained via the mode shape of the membrane resonator [16]. Due to the introduction of photonic crystal structure, the effective mass of the membrane resonator changes from 9.48 ng to 15.19 ng.

2.2.3. Optomechanical cooperativity

High optomechanical cooperativity is crucial to the optomechanical systems and their applications [27]. The optomechanical cooperativity C in cavity optomechanical systems is defined as

$$C \equiv \frac{4g_0^2 n_c}{\kappa \Gamma_m}, \tag{4}$$

where

$$g_0 = G x_{\text{zpf}}, \quad x_{\text{zpf}} = \sqrt{\frac{\hbar}{2 m_{\text{eff}} \Omega_m}}, \tag{5}$$

where g_0 is the single-photon optomechanical coupling rate, n_c is the mean number of photons in the optomechnical cavity, κ is the decay rate of the optical cavity, and Γ_m is the decay rate of the mechanical energy, G is the light frequency shift per unit displacement, x_{zpf} is the zero-point fluctuations, and $\Omega_m = 2\pi\omega_m$ is the angular frequency of the mechanical resonator. From Eq. (4),

Optics EXPRESS

it is evident that a high finesse cavity, low effective mass, and high mechanical quality are critical to achieve a high optomechanical cooperativity C.

The optomechanical cooperativity can be expressed as the single-photon cooperativity C_0 enhanced by the intra-cavity mean number of photons n_c

$$C = C_0 n_c, \quad C_0 = \frac{4g_0^2}{\kappa\Gamma_m} = \frac{16\pi c x_{\mathrm{zpf}}^2 F}{L\lambda^2\Gamma_m}, \tag{6}$$

where c is the speed of light, F and L are the finesse and length of the cavity, respectively, λ is the wavelength of the light field. Note that optomechanical systems with large single-photon cooperativity might enable implementation of nonlinear optomechanical schemes for non-classical state generation, such as photon antibunching [27]. By employing the presented phononically shielded multi-wavelength photonic-crystal membrane as the end mirror in a Fabry-Perot-type optomechanical system and using the simulated parameters of $x_{\mathrm{zpf}} = 6.54 \times 10^{-16}$ m, $F = 1.53 \times 10^4$, $\lambda = 1566.3$ nm, $\Gamma_m = 2.99 \times 10^{-3}$ Hz, and a short cavity length of $L = 2$ μm, we can expect a theoretical single-photon cooperativity of $C_0 \sim 6.86 \times 10^3$ at room temperature.

2.2.4. Effects of fabrication error and finite beam waist

Notice that the fabrication errors of the photonic crystal structure can affect the performance of the membrane resonator. For a fabrication error of +5 (−5) nm in the etched thickness of the membrane, the results of the numerical simulation show that the band gap remains almost unchanged. The intrinsic frequency of the lowest-order mechanical defect mode becomes 1.34 (1.35) MHz, and the peak reflectivity changes to 99.62% at 860.08 nm (99.63% at 847.13 nm), 99.97% at 1054.8 nm (99.97% at 1054 nm), and 99.96% at 1578.3 nm (99.97% at 1554.5 nm), respectively. On the other hand, the experimentally realized finesses are often lower than the theoretical predictions. [11].

In above simulations, a plane wave at normal incidence and infinite extension of the photonic crystal structure is adopted. For real devices, the beam waist of the incident light field is finite, which induces a range of wave vectors and can lead to reduced reflectivity [16]. Due to the limited photonic crystal mirror diameter, a larger beam waist will cause excess clipping loss, and a smaller beam waist will lead to low reflectivity arising from the broader angular spectrum. Therefore, there exists an optimal compromise for the beam waist.

3. Potential applications

The presented phononically shielded multi-wavelength photonic-crystal membrane can interact with the optical cavity mode at different wavelengths via radiation pressure. This optomechanical interface can be employed to measure the optomechanical entanglement [28], and achieve the optical wavelength conversion of quantum states [29]. For both applications, a two-cavity optomechanical system is required, as shown in Fig. 5. It is configured by two fixed end mirrors and a movable membrane mirror in the middle that also acts as the mechanical resonator. The first mirror on the left and the membrane mirror form the first Fabry-Perot cavity C_1, and the second mirror on the right combined with the membrane mirror forms a second Fabry-Perot cavity C_2.

To measure the optomechanical entanglement between the membrane resonator and the cavity field $\hat{a}_{\lambda_1}$ of C_1 at wavelength λ_1, the quantum state of the mechanical mode is firstly mapped to an optical mode $\hat{a}_{\lambda_2}$ in C_2 via optomechanical interaction. In this case, both the position and the momentum of the membrane resonator can be measured by detecting the output field of C_2 at wavelength λ_2. Then, the quantum correlations between the two output fields of cavity C_1 and C_2 are measured to characterize the optomechanical entanglement through the logarithmic negativity E_N [30].

Optics EXPRESS

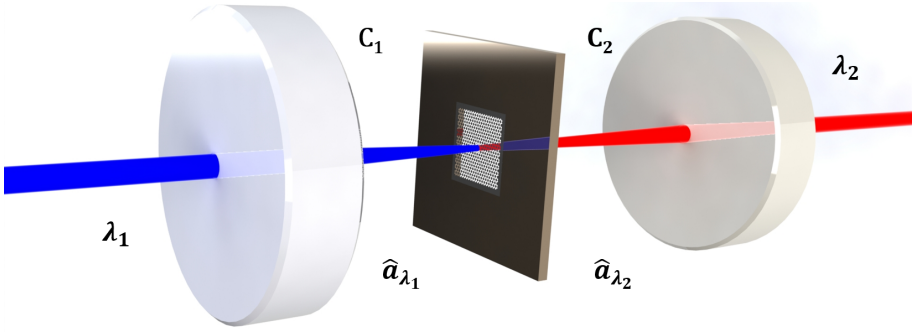

Fig. 5. Schematic diagram of the two-cavity optomechanical system. It consists of two fixed mirrors and a movable membrane in the middle. The first mirror on the left and the membrane constitutes the Fabry-Perot cavity C_1, the second mirror on the right and the membrane forms the second Fabry-Perot cavity C_2.

For the optical wavelength conversion of quantum states [29], the membrane resonator acts as an interface through which the quantum state is converted between different wavelengths of light fields. More precisely, we can map the quantum state of the optical field $\hat{a}_{\lambda_1}$ at wavelength λ_1 to the mechanical state, which in turn can be mapped to the quantum state of the optical field $\hat{a}_{\lambda_2}$ at wavelength λ_2.

The advantages of the optomechanical wavelength conversion are that the conversion can be achieved at very low pump power and no phase-matching conditions must be met. However, the mechanical resonator should be cooled close to the ground state to suppress the effect of the thermal phonon noise, and the conversion bandwidth is limited by the frequency of the mechanical resonator. The advantages of the nonlinear optical frequency conversion are that no vacuum and cryogenic temperature are required, and the conversion bandwidth is determined by the phase-matching bandwidth, which is relatively wider. The disadvantage is that it needs relatively strong pump power and satisfy the phase-matching conditions.

The presented phononically shielded multi-wavelength photonic-crystal membrane can also be applied to the microwave-optical conversion [31] and acceleration sensing [32]. For the former one, our designed membrane can serve as both the mechanical resonator and one of the end mirrors of the optical resonator to enable a conversion of the microwave to optical fields with different light carriers. Furthermore, the high mechanical quality factor and optical reflectivity are beneficial to improve the conversion efficiency and suppress the vibration noise. For the latter one, the acceleration sensitivity can be significantly boosted by replacing the trampoline membrane with the designed high mechanical quality factor and optical reflectivity membrane, and the other unpatterned membrane with the photonic-crystal membrane. The multi-wavelength operation can increase the usability and flexibility of the optomechanical accelerometry.

4. Conclusions

We have proposed a phononically shielded multi-wavelength photonic-crystal SiN membrane for cavity quantum optomechanics. The membrane resonator features highly reflectivity at multi-wavelengths and high mechanical quality factor. The designed devices can be exploited to construct a compact optomechanical system with high optomechanical cooperativity. It may find useful applications in cavity optomechanics to realize quantum frequency conversion, measurement of optomechanical entanglement, microwave-optical conversion, acceleration sensing, and other quantum information applications. In our future work, we will fabricate the designed membrane resonator and verify its optical and mechanical properties.

Optics EXPRESS

Funding. National Natural Science Foundation of China (11774209, 11804208, 12174232).

Disclosures. The authors declare no conflicts of interest.

Data availability. Data underlying the results presented in this paper are not publicly available at this time but may be obtained from the authors upon reasonable request.

References

1. M. Aspelmeyer, T. J. Kippenberg, and F. Marquardt, eds., "Cavity optomechanics: Nano- and micromechanical resonators interacting with light," (Springer Berlin Heidelberg, 2014).
2. W. P. Bowen, "Quantum optomechanics," 1st ed. (CRC University, 2015).
3. S. Barzanjeh, A. Xuereb, S. Gröblacher, *et al.*, "Optomechanics for quantum technologies," Nat. Phys. **18**(1), 15–24 (2022).
4. A. M. Jayich, J. C. Sankey, B. M. Zwickl, *et al.*, "Dispersive optomechanics: a membrane inside a cavity," New J. Phys. **10**(9), 095008 (2008).
5. J. D. Joannopoulos, J. N. Winn, and S. G. Johnson, "Photonic crystals: Molding the flow of light - second edition," (Princeton University, 2011).
6. K. Sakoda, "Optical properties of photonic crystals," 2nd ed., Springer Series in Optical Sciences No. 80 (Springer, 2005).
7. V. Lousse, W. Suh, O. Kilic, *et al.*, "Angular and polarization properties of a photonic crystal slab mirror," Opt. Express **12**(8), 1575–1582 (2004).
8. S. Fan and J. D. Joannopoulos, "Analysis of guided resonances in photonic crystal slabs," Phys. Rev. B **65**(23), 235112 (2002).
9. C. H. Bui, J. Zheng, S. W. Hoch, *et al.*, "High-reflectivity, high-Q micromechanical membranes via guided resonances for enhanced optomechanical coupling," Appl. Phys. Lett. **100**(2), 021110 (2012).
10. S. Kini Manjeshwar, K. Elkhouly, J. M. Fitzgerald, *et al.*, "Suspended photonic crystal membranes in AlGaAs heterostructures for integrated multi-element optomechanics," Appl. Phys. Lett. **116**(26), 264001 (2020).
11. F. Zhou, Y. Bao, J. J. Gorman, *et al.*, "Cavity optomechanical bistability with an ultrahigh reflectivity photonic crystal membrane," Laser Photonics Rev. **17**(10), 2300008 (2023).
12. R. A. Norte, J. P. Moura, and S. Gröblacher, "Mechanical resonators for quantum optomechanics experiments at room temperature," Phys. Rev. Lett. **116**(14), 147202 (2016).
13. T. Antoni, A. G. Kuhn, T. Briant, *et al.*, "Deformable two-dimensional photonic crystal slab for cavity optomechanics," Opt. Lett. **36**(17), 3434–3436 (2011).
14. A. R. Agrawal, J. P. Manley, D. Allepuz-Requena, *et al.*, "A suspended focusing Si_3N_4 metamirror for integrated cavity optomechanics," in *Frontiers in Optics + Laser Science 2023 (FiO, LS)* (Optica Publishing Group, 2023), paper FTh3B.4.
15. J. P. Moura, R. A. Norte, J. Guo, *et al.*, "Centimeter-scale suspended photonic crystal mirrors," Opt. Express **26**(2), 1895–1909 (2018).
16. G. Enzian, Z. Wang, A. Simonsen, *et al.*, "Phononically shielded photonic-crystal mirror membranes for cavity quantum optomechanics," Opt. Express **31**(8), 13040–13052 (2023).
17. A. R. Agrawal, J. Manley, D. Allepuz-Requena, *et al.*, "Focusing membrane metamirrors for integrated cavity optomechanics," Optica **11**(9), 1235–1241 (2024).
18. F. Zhou, Y. Bao, J. J. Gorman, *et al.*, "Ultrahigh reflectivity photonic crystal membranes with optimal geometry," APL Photonics **9**(7), 076120 (2024).
19. Y. Tsaturyan, A. Barg, E. S. Polzik, *et al.*, "Ultracoherent nanomechanical resonators via soft clamping and dissipation dilution," Nat. Nanotech. **12**(8), 776–783 (2017).
20. Z. Wang, E. S. Polzik, and D. G. Enzian, "Characterization of high-Q ultralight membranes towards novel optomechanical designs, Univ. Copenhagen, 2022.," Nat. Phys. **603**(7901), E15–E16 (2022).
21. D. F. Santos, A. Guerreiro, and J. M. Baptista, "Numerical investigation of a refractive index SPR D-type optical fiber sensor using COMSOL multiphysics," Photonic Sens. **3**(1), 61–66 (2013).
22. H. R. Philipp, "Optical properties of silicon nitride," J. Electrochem. Soc. **120**(2), 295–300 (1973).
23. Y. Tsaturyan, A. Barg, A. Simonsen, *et al.*, "Demonstration of suppressed phonon tunneling losses in phononic bandgap shielded membrane resonators for high-Q optomechanics," Opt. Express **22**(6), 6810–6821 (2014).
24. C. Reetz, R. Fischer, G. G. T. Assumpç ao, *et al.*, "Analysis of membrane phononic crystals with wide band gaps and low-mass defects," Phys. Rev. Appl. **12**(4), 044027 (2019).
25. D. S. Bindel and S. Govindjee, "Elastic PMLs for resonator anchor loss simulation," Int. J. Numer. Meth. Eng. **64**(6), 789–818 (2005).
26. A. Frangi, A. Bugada, M. Martello, *et al.*, "Validation of PML-based models for the evaluation of anchor dissipation in MEMS resonators," Eur. J. Mech. A Solids **37**, 256–265 (2013).
27. K. Børkje, "Critical quantum fluctuations and photon antibunching in optomechanical systems with large single-photon cooperativity," Phys. Rev. A **101**(5), 053833 (2020).
28. J. Chen, M. Rossi, D. Mason, *et al.*, "Entanglement of propagating optical modes via a mechanical interface," Nat. Commun. **11**(1), 943 (2020).

Optics EXPRESS

29. L. Tian and H. Wang, "Optical wavelength conversion of quantum states with optomechanics," Phys. Rev. A **82**(5), 053806 (2010).
30. D. Vitali, S. Gigan, A. Ferreira, *et al.*, "Optomechanical entanglement between a movable mirror and a cavity field," Phys. Rev. Lett. **98**(3), 030405 (2007).
31. R. W. Andrews, R. W. Peterson, T. P. Purdy, *et al.*, "Bidirectional and efficient conversion between microwave and optical light," Nat. Phys. **10**(4), 321–326 (2014).
32. M. D. Chowdhury, A. R. Agrawal, and D. J. Wilson, "Membrane-based optomechanical accelerometry," Phys. Rev. Appl. **19**(2), 024011 (2023).